Title of Literature Review: Generative AI for Medical X-ray Image Synthesis using Transformers, LoRA, & Diffusion Models

Fahad M Mujawar, Student ID: 20711746

Introduction & Motivation

Medical imaging is vital for diagnostics, treatment planning, and disease monitoring. However, access to diverse, high-quality data remains limited due to privacy regulations, acquisition costs, and annotation challenges. [1][2] Generative AI models—such as GANs, diffusion models, and transformers—offer solutions by synthesizing realistic images that support data augmentation, rare condition simulation, and medical training.

This review explores state-of-the-art generative AI techniques applied to medical X-ray synthesis, with supporting examples from MRI and CT. Emphasis is placed on parameter-efficient fine-tuning methods like LoRA, enabling deployment in low-resource environments. Key challenges, including clinical validation, anatomical realism, and ethical concerns, are discussed alongside current opportunities in this evolving field.

1.1 Research Field Challenges

1. **Data Availability & Privacy:** Medical data is subject to regulatory constraints such as HIPAA & GDPR, limiting the size & diversity of accessible datasets [1][2][3][5]
2. **Clinical Validity of Synthesized Data:** Synthetic images must retain diagnostic value; however, many models optimize for visual realism rather than clinical significance [1][2][5][10]
3. **Computational Burden:** Transformer & diffusion models often require large memory footprints & long training cycles [5][7][9][10]
4. **Ethical & Regulatory Standards:** Adoption in clinical practice necessitates strict ethical oversight & validation through peer-reviewed medical trials[1][5][9]

1.2 Survey Scope

This review covers peer-reviewed literature on generative models applied to medical imaging, specifically X-ray, MRI, & CT image synthesis. We include studies utilizing GANs, transformers, & diffusion models with a focus on parameter-efficient techniques such as LoRA. Excluded are preprints (e.g., arXiv-only submissions), purely discriminative tasks (e.g., segmentation/classification), & traditional non-AI approaches. The selected literature includes both foundational & recent works published in indexed journals or conference proceedings with DOIs.

1.3 Search Methodology

Supervised by **Dr. Ulrik Torben Buchholtz**, I initiated the literature review in April 2025. Our meetings & discussions led to an initial search centered around GAN-based augmentation in radiology. Key databases queried included PubMed, IEEE Xplore, SpringerLink, & ScienceDirect. Search terms included: "medical image synthesis", "GAN X-ray augmentation", "transformer MRI generation", "LoRA diffusion models". The survey paper by Yi et al. (2019) was selected for foundational context.[1]

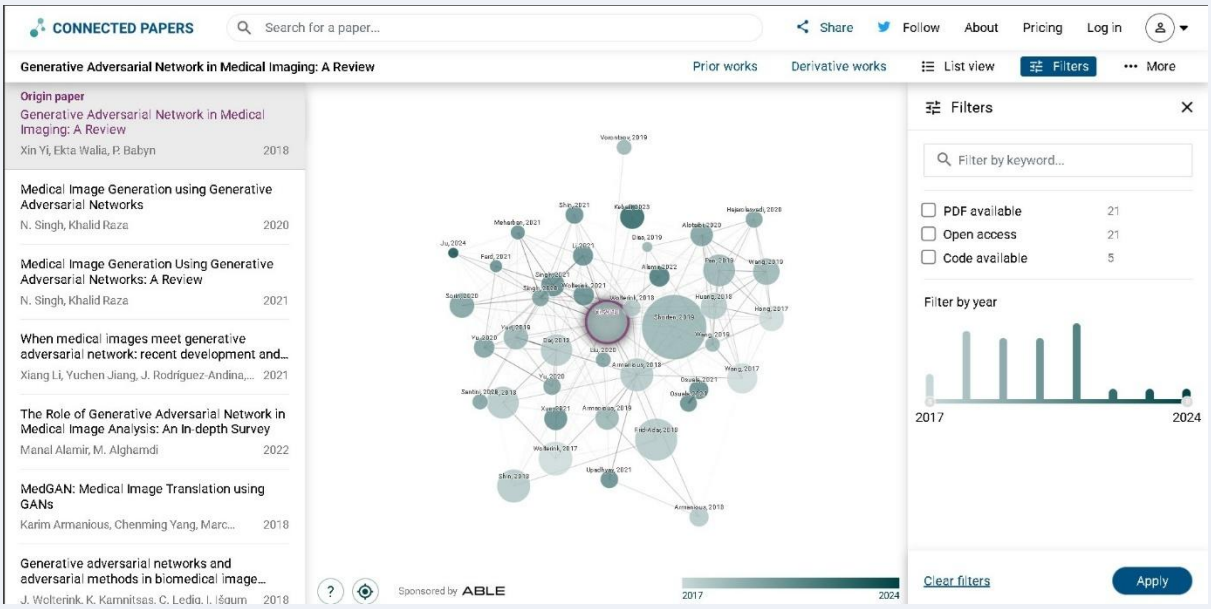

Figure 1. Screenshot from ConnectedPapers.com with Yi et al. (2019) highlighted.

https://www.connectedpapers.com/main/3009807383d99aeae77cff2cd1487e28a60a543c/Generative-Adversarial-Network-in-Medical-Imaging%3A-A-Review/graph

1.4 Classification of Literature & Organization

We categorize the ten reviewed papers into three major groups: *GAN-based Models*, *Diffusion Models*, and *Transformers & LoRA*. This classification reflects both methodological commonalities and emerging paradigms in medical image synthesis. Each category addresses similar challenges—data scarcity, quality, and clinical realism—but approaches them with differing computational strategies. This organization mirrors the research trajectory from early adversarial training to scalable transformers and sample-efficient diffusion-based approaches.

The papers are presented in ascending order of model complexity and relevance to current trends. GANs are placed first due to their historical prominence, followed by diffusion models which overcome GAN limitations, and finally Transformer & LoRA-based works that reflect recent innovations in scalability and alignment. This ordering supports an evolutionary view of the field and facilitates understanding of methodological shifts across medical image generation tasks.

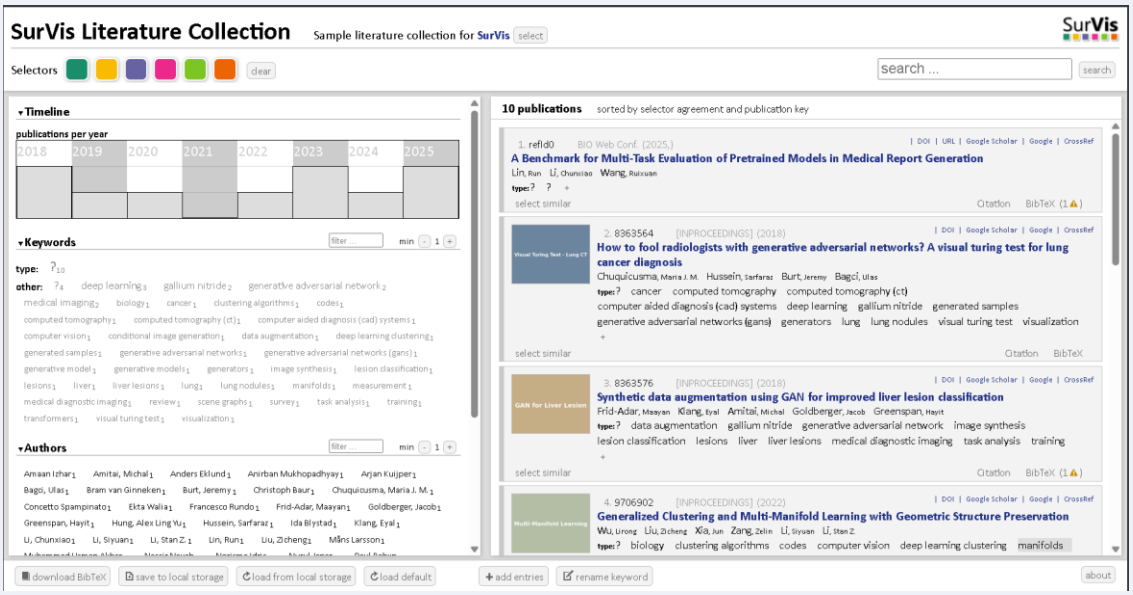

Figure 2. Survis review. https://fahadmujawar.github.io/Survis-litreview/src/index.html [11]

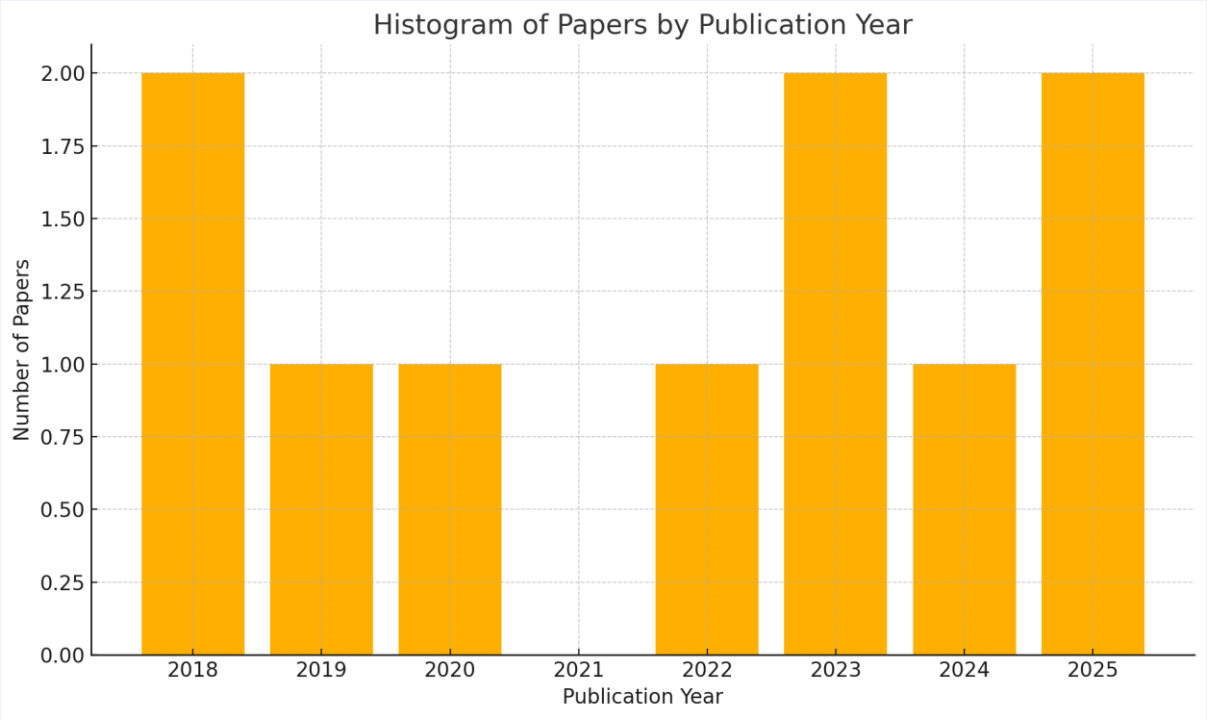

Figure 3. Histogram of Paper Publications by Year

Table 1. Classification of Reviewed Papers

Category	Paper No.	Summary Topic
GAN-based Models	Paper 1	Survey of GANs in medical image reconstruction
	Paper 2	DC-GAN-based lung nodule generation evaluated via Visual Turing Test
	Paper 3	GAN-based synthetic augmentation for liver lesion classification
	Paper 4	Survey of GANs across seven medical imaging tasks including synthesis and segmentation
Diffusion Models	Paper 5	Comparison of GANs and diffusion models for MRI tumor segmentation
	Paper 6	Med-cDiff: Conditional diffusion for X-ray denoising, MRI super-resolution, and inpainting
	Paper 7	Benchmarking PEFT + LoRA medical foundation models across multiple modalities
Transformers and LoRA	Paper 8	Transformer-based image generation from scene graphs using SGTransformer and VQVAE
	Paper 9	Radiology report generation using multi-modal Transformer + Phi-3 Mini via ORPO
	Paper 10	GCML: Transformer-driven manifold learning for clustering and data structuring

2. Paper Summaries

Survey Paper

(Paper 1)

What: Topic Overview

This paper presents a comprehensive survey on the application of Generative Adversarial Networks (GANs) in the field of medical imaging. GANs are a class of deep generative models where a generator & discriminator compete in a zero-sum game to synthesize realistic data. The survey systematically reviews GAN applications across a wide range of tasks in medical image analysis.

Why: Importance of the Field

The medical imaging domain faces challenges like limited labeled data, domain shift between modalities or institutions, & privacy restrictions. GANs offer solutions through data augmentation, cross-modality synthesis, anomaly detection, segmentation regularization, & more. Their generative capability makes them valuable for enhancing dataset diversity & enabling unsupervised or weakly-supervised learning.

How: Paper Classification & Contributions

The survey categorizes GAN applications into six canonical medical imaging tasks:

1. Reconstruction (e.g., low-dose CT, MR denoising)
2. Image Synthesis (e.g., cross-modality, rare disease augmentation)
3. Segmentation (using adversarial shape constraints)
4. Classification (semi-supervised learning, domain adaptation)
5. Detection (e.g., unsupervised lesion detection)
6. Registration (image alignment using learned transformations)

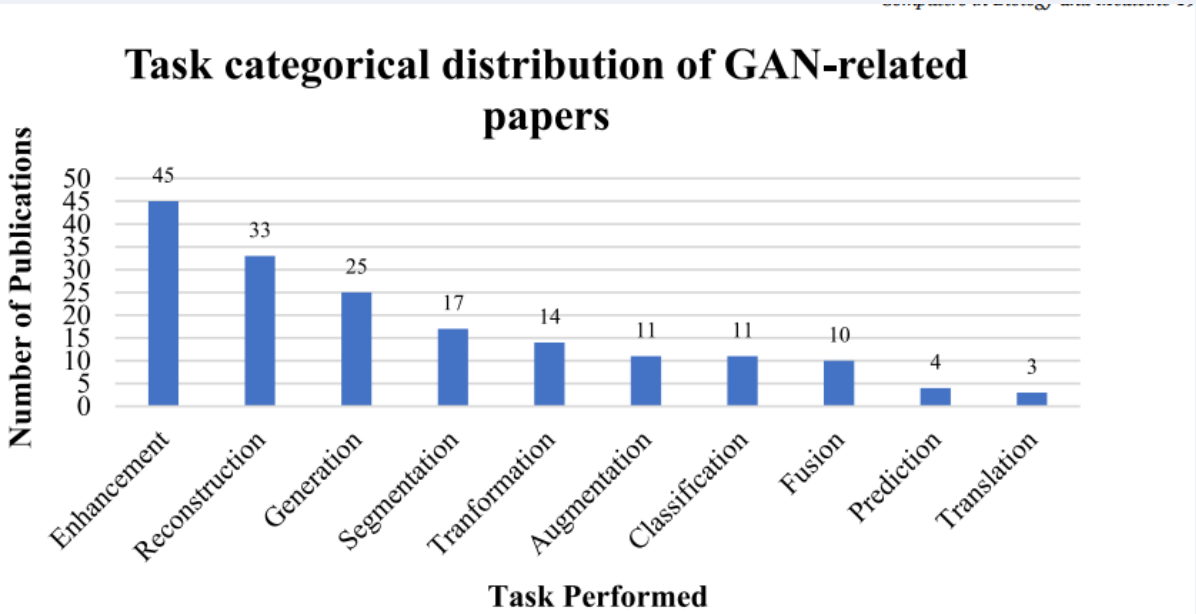

Figure4. Task-based categorical distribution of GAN related articles.[1]

This work further organizes reviewed studies by:

- GAN architecture variants (e.g., pix2pix, CycleGAN, WGAN, PGGAN)
- Loss functions used (L1, perceptual, adversarial, saliency)
- Data modality (MRI, CT, PET, X-ray, fundus, histopathology)
- Supervision level (paired/unpaired, semi-supervised, unsupervised)

The paper presents extensive tables summarizing 200+ publications, datasets used, & performance metrics. It also discusses challenges such as hallucination in unpaired synthesis, lack of reliable evaluation metrics, & overfitting in low-data regimes.[1]

2.1 GAN-based Models

(Paper 2) This paper uses DC-GANs to generate synthetic lung nodules for evaluating realism via a Visual Turing test. Two radiologists assessed generated nodules (benign, malignant, & mixed) to determine their authenticity. Results demonstrate that realistic GAN-generated nodules can deceive experts, supporting their utility in education & dataset augmentation.

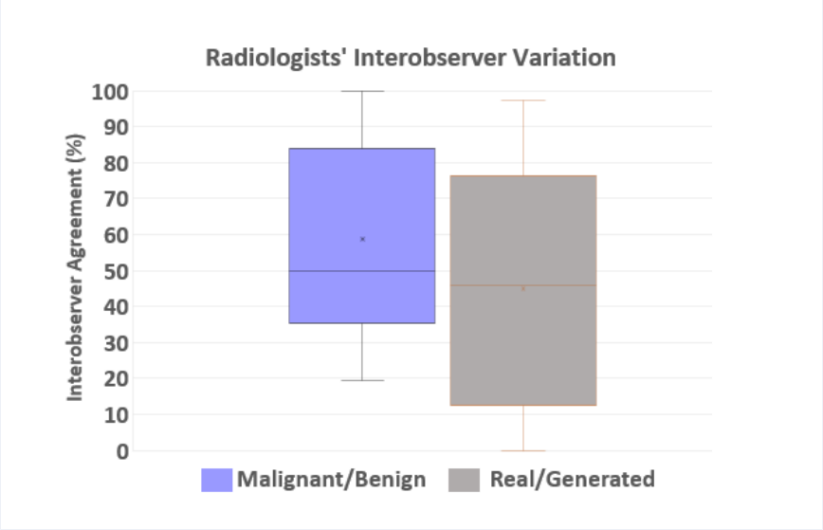

Figure 5. Radiologists' inter-observer variation for the respective cases[2]

Qualitative & quantitative evaluation - Visual Turing Tests. Metrics include False Recognition Rate (FRR), True Recognition Rate (TRR), & inter-observer agreement.

Evaluating & Backing Findings

Radiologists reviewed 18 blinded experiments comparing real vs. generated nodules. Accuracy in identifying fake images quantified visual realism. Inter-observer variation measured agreement on malignancy & authenticity, validating image quality.[2]

(Paper 3) This paper presents a method combining classical & GAN-based synthetic augmentation to enhance liver lesion classification from CT images. Using DCGANs, class-specific lesions are generated to supplement limited real data. Incorporating synthetic samples improved sensitivity from 78.6% to 85.7% & specificity from 88.4% to 92.4%, validating the augmentation's impact

Quantitative evaluation using classification accuracy, sensitivity, specificity, & confusion matrices. Expert radiologists also assessed real versus synthetic lesions.

Evaluating & Backing Findings

CNNs were trained with & without synthetic data across three folds. Performance gains were measured on held-out sets. Radiologists classified real & generated lesions, achieving similar accuracy, confirming clinical realism of the synthetic images.[3]

.

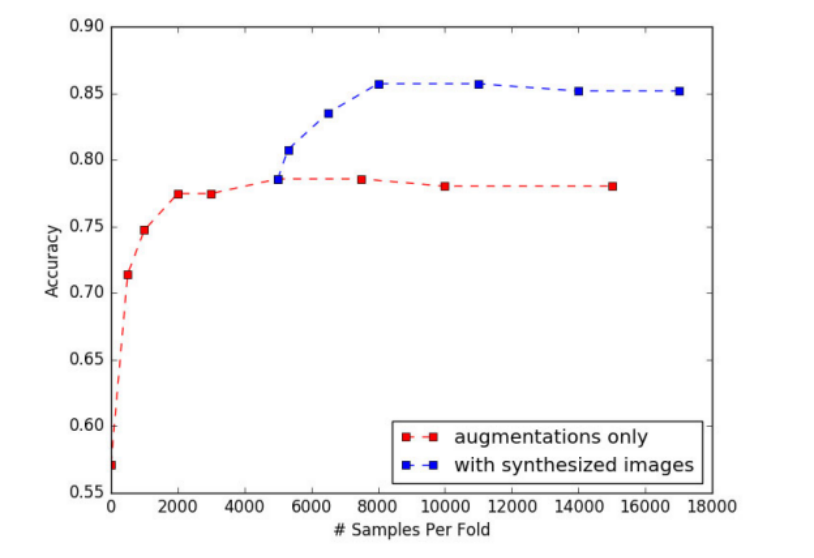

Figure 6. Accuracy results for liver lesion classification [3]

(Paper 4) This state-of-the-art survey reviews 79 papers on GAN-based methods in medical image analysis across seven tasks: synthesis, segmentation, reconstruction, detection, de-noising, registration, & classification. It highlights GAN variants, application-specific challenges, & architectural innovations, offering a structured categorization of modalities & techniques, alongside key insights on performance metrics.

This is a **quantitative literature review**, providing **task-based tabular comparisons**. It uses metric analysis & code availability as benchmarks, without introducing new experimental data.

Registration GAN-based methods in medical image processing.

Method	Arch	Loss	Modality	Dataset	Performance	PR	Code
[108]	U-net, GAN	Adv, Regular	MRI 3D Brain	LPBA40 IBSR18 CUMC12 MGH10 Train: 30 Test: 10	DSC = 71.8 ± 2.3% DSC = 57.8 ± 2.7% DSC = 54.4 ± 2.9% DSC = 61.7 ± 2.1%	Yes	No
[7]	CNN, WGAN	Adv	Prostate 3D MRI and TRUS	Unknown Train: 636 Test: 127	TRE = 3.84 mm DSC = 0.58	Yes	No
[109]	3D GAN	Adv, DSC, Regular	Prostate 3D MRI TRUS	Unknown 108 pairs	TRE = 6.3 mm DSC = 0.82	Yes	No

Figure 7. Screenshot of Table showing tabular-comparisions[4]

Evaluating & Backing Findings

Evaluation included categorizing peer-reviewed & preprint papers, organizing metrics & architectures, & analyzing method effectiveness per task. Visual examples, dataset types, & performance summaries support comparative insights[4]

2.2 Diffusion Models

(Paper 5) This study compares four GANs and a diffusion model for generating brain tumor MRIs, evaluated via Dice, Hausdorff, FID, and expert review. Diffusion outperformed others but showed signs of memorization, raising privacy concerns. Synthetic-trained models achieved up to 91–100% of real-image segmentation performance.

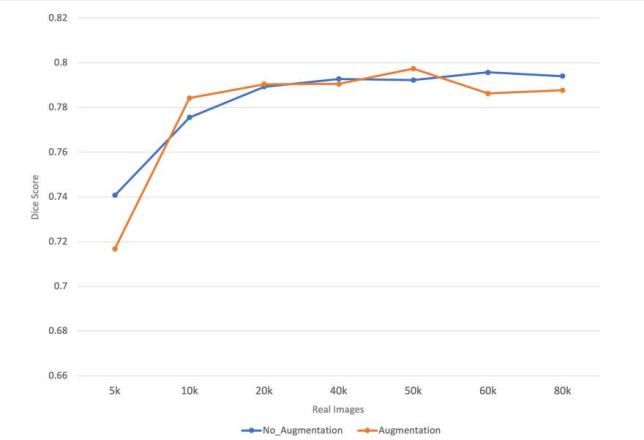

Figure 8.Graph depicting the U-Net segmentation performance (Dice score)[5]

Evaluating & Backing Findings

Evaluations included training segmentation models on synthetic datasets, visual assessment by a neuroradiologist, & memorization checks via image similarity. Metrics like Dice & FID quantified realism & segmentation quality.[5]

(Paper 6) Med-cDiff introduces a conditional diffusion model for medical image generation across tasks like MRI super-resolution, X-ray denoising, & inpainting. It consistently **outperforms GAN & VAE-based models** in image quality, sharpness, & utility for downstream tasks. The model demonstrates generalizability across modalities without needing task-specific adaptation or architecture changes.

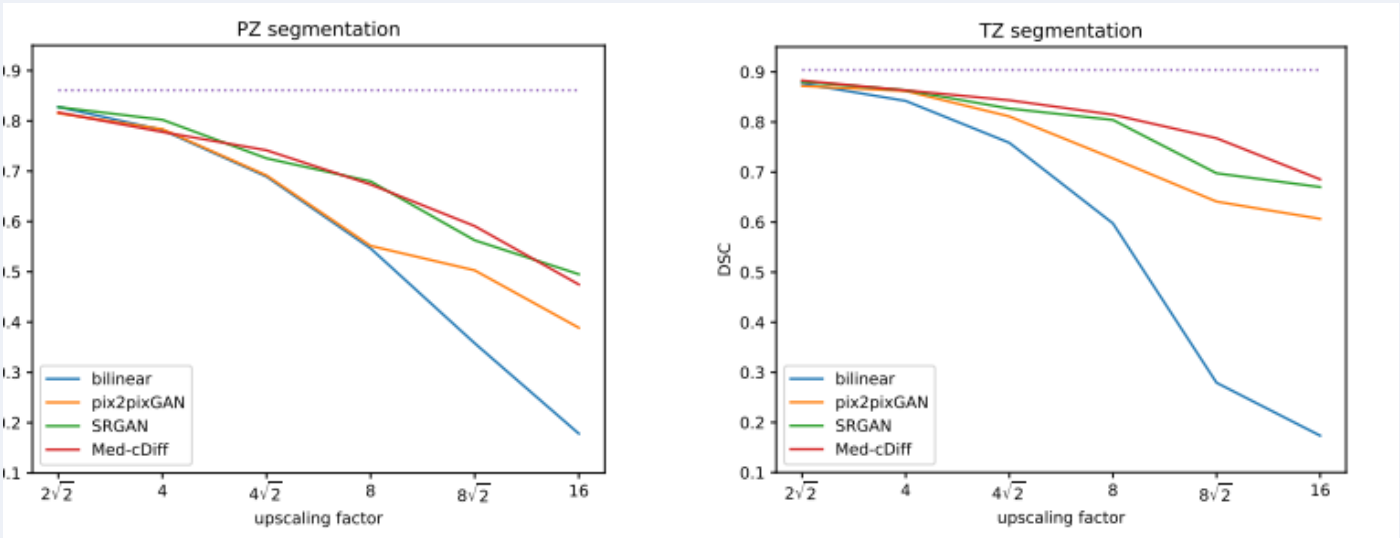

Figure 9. Graphs illustrating Med-CDiff outperforming other models[6]

Quantitative evaluation includes LPIPS, FID, classification accuracy, Dice scores, & 2AFC perception tests. Qualitative analysis compares visual fidelity across methods. Downstream tasks like segmentation & classification test model utility.

Evaluating & Backing Findings

The authors benchmarked Med-cDiff on three imaging tasks using real clinical datasets. Results were validated using standard metrics & expert-annotated evaluations, supported by comparisons to state-of-the-art GAN-based & VAE-based methods across conditions & modalities[6]

(Paper 7) This paper presents a new benchmark for evaluating medical report generation (MRG) across four modalities—CT, X-ray, ultrasound, & pathology. Using PEFT & LoRA with pretrained models, the study shows that medical foundation models outperform modality-specific & natural domain models, particularly in cross-modal tasks. GPT-4o augmented dataset ensures uniformity.

Quantitative metrics include **BERTScore**, ROUGE-L, BLEU, METEOR, & CIDEr. Statistical significance is assessed via confidence intervals & p-values. No qualitative evaluation is reported.

BERTScore of the **Best model** and other models.

Index	Method	CT					X-Ray					Ultrasound					Pathology				
		BS	R	B1	C	M	BS	R	B1	C	M	BS	R	B1	C	M	BS	R	B1	C	M
#01	R2GenGPT	*0.622* (0.616, 0.628)	0.207 (0.198, 0.216)	0.251 (0.246, 0.257)	0.127 (0.122, 0.131)	0.097 (0.092, 0.102)	0.630 (0.626, 0.635)	0.195 (0.189, 0.201)	0.229 (0.221, 0.237)	0.166 (0.158, 0.173)	0.091 (0.087, 0.096)	0.621 (0.615, 0.627)	0.183 (0.176, 0.191)	0.201 (0.194, 0.208)	0.097 (0.088, 0.106)	0.077 (0.072, 0.083)	*0.819* (0.814, 0.825)	0.545 (0.537, 0.553)	0.610 (0.602, 0.619)	2.998 (2.948, 3.041)	0.346 (0.339, 0.353)
	Nature	*0.626* (0.622, 0.631)	0.215 (0.208, 0.221)	0.258 (0.252, 0.265)	0.147 (0.143, 0.151)	0.103 (0.099, 0.107)	*0.623* (0.617, 0.628)	0.194 (0.187, 0.200)	0.217 (0.209, 0.226)	0.147 (0.140, 0.155)	0.086 (0.081, 0.092)	0.625 (0.621, 0.630)	0.193 (0.187, 0.198)	0.218 (0.212, 0.225)	0.119 (0.111, 0.126)	0.083 (0.078, 0.088)	*0.825* (0.819, 0.830)	0.547 (0.540, 0.554)	0.618 (0.611, 0.625)	3.108 (3.065, 3.151)	0.350 (0.344, 0.357)
	XrayGPT	*0.623* (0.617, 0.629)	0.209 (0.202, 0.216)	0.246 (0.240, 0.251)	0.134 (0.128, 0.139)	0.096 (0.091, 0.100)	**0.632** (0.628, 0.635)	0.207 (0.204, 0.212)	**0.231** (0.224, 0.238)	0.174 (0.166, 0.181)	0.098 (0.094, 0.103)	0.621 (0.617, 0.627)	0.191 (0.185, 0.197)	0.207 (0.201, 0.214)	0.104 (0.096, 0.113)	0.075 (0.071, 0.080)	*0.815* (0.810, 0.821)	0.522 (0.513, 0.531)	0.611 (0.603, 0.619)	2.824 (2.758, 2.890)	0.339 (0.332, 0.346)
	Nature	*0.624* (0.619, 0.629)	0.212 (0.207, 0.218)	0.252 (0.247, 0.258)	0.142 (0.138, 0.147)	0.098 (0.094, 0.101)	*0.625* (0.621, 0.628)	0.201 (0.195, 0.207)	0.210 (0.201, 0.218)	0.152 (0.145, 0.160)	0.092 (0.086, 0.097)	0.622 (0.618, 0.628)	0.194 (0.188, 0.200)	0.216 (0.209, 0.222)	0.116 (0.109, 0.223)	0.081 (0.075, 0.087)	*0.822* (0.816, 0.828)	0.534 (0.526, 0.542)	0.617 (0.610, 0.625)	2.985 (2.926, 3.044)	0.346 (0.339, 0.350)
#02	USFM	*0.614* (0.610, 0.619)	0.197 (0.189, 0.204)	0.237 (0.232, 0.243)	0.114 (0.109, 0.118)	0.092 (0.089, 0.095)	*0.617* (0.614, 0.621)	0.185 (0.180, 0.191)	0.194 (0.187, 0.202)	0.121 (0.114, 0.127)	0.074 (0.068, 0.079)	0.624 (0.618, 0.629)	0.184 (0.177, 0.194)	0.213 (0.206, 0.221)	0.113 (0.107, 0.121)	0.082 (0.076, 0.087)	*0.806* (0.799, 0.813)	0.517 (0.508, 0.526)	0.581 (0.572, 0.591)	2.160 (2.096, 2.224)	0.302 (0.292, 0.312)
	Nature	*0.621* (0.615, 0.627)	0.204 (0.197, 0.212)	0.245 (0.239, 0.251)	0.125 (0.119, 0.130)	0.097 (0.093, 0.101)	*0.620* (0.615, 0.624)	0.187 (0.181, 0.192)	0.203 (0.195, 0.211)	0.132 (0.125, 0.138)	0.081 (0.076, 0.086)	0.621 (0.615, 0.626)	0.181 (0.174, 0.187)	0.194 (0.187, 0.201)	0.092 (0.081, 0.102)	0.075 (0.069, 0.081)	*0.812* (0.805, 0.820)	0.523 (0.514, 0.532)	0.588 (0.578, 0.597)	2.427 (2.332, 2.525)	0.314 (0.303, 0.324)
#03	PLIP	*0.619* (0.612, 0.625)	0.204 (0.198, 0.211)	0.226 (0.221, 0.232)	0.121 (0.116, 0.127)	0.094 (0.089, 0.099)	*0.621* (0.616, 0.627)	0.189 (0.183, 0.194)	0.210 (0.201, 0.219)	0.144 (0.136, 0.151)	0.095 (0.089, 0.101)	*0.618* (0.613, 0.624)	0.188 (0.181, 0.194)	0.210 (0.203, 0.218)	0.117 (0.109, 0.126)	0.082 (0.076, 0.089)	**0.839** (0.835, 0.844)	**0.599** (0.591, 0.607)	**0.643** (0.636, 0.649)	3.320 (3.287, 3.353)	**0.368** (0.361, 0.375)
	Nature	-	-	-	-	-	-	-	-	-	-	-	-	-	-	-	-	-	-	-	-
#04	Bio-MedCLIP	**0.632** (0.628, 0.637)	**0.223** (0.216, 0.230)	**0.271** (0.265, 0.274)	**0.205** (0.197, 0.213)	**0.117** (0.112, 0.123)	0.628 (0.625, 0.634)	**0.211** (0.206, 0.215)	0.227 (0.221, 0.234)	**0.174** (0.167, 0.181)	**0.104** (0.098, 0.111)	**0.625** (0.620, 0.629)	**0.198** (0.194, 0.203)	**0.234** (0.228, 0.239)	**0.133** (0.125, 0.141)	**0.093** (0.087, 0.099)	0.832 (0.826, 0.837)	0.593 (0.586, 0.601)	0.635 (0.629, 0.641)	**3.407** (3.374, 3.442)	0.358 (0.349, 0.366)
	Nature	0.625 (0.619, 0.632)	0.206 (0.198, 0.214)	0.232 (0.226, 0.239)	0.146 (0.139, 0.154)	0.096 (0.091, 0.112)	*0.623* (0.619, 0.628)	0.191 (0.184, 0.197)	0.217 (0.209, 0.225)	0.146 (0.138, 0.155)	0.098 (0.092, 0.105)	0.621 (0.617, 0.625)	0.190 (0.184, 0.195)	0.212 (0.205, 0.221)	0.115 (0.104, 0.126)	0.084 (0.075, 0.092)	*0.815* (0.808, 0.823)	0.533 (0.522, 0.543)	0.579 (0.565, 0.592)	2.529 (2.405, 2.653)	0.318 (0.311, 0.325)

Figure.10 Screenshot of table depicting BERTScore[7]

Evaluating & Backing Findings

They fine-tuned & compared pretrained models on a balanced multi-modality dataset. Experiments measured model generalization across tasks. Statistical tests & reproducibility via random seeds supported the findings.[7]

2.3 Transformers & LoRA-Based Models

Paper 8) This study introduces a fully transformer-based model for generating images from scene graphs. It replaces GANs with stable transformer architectures, using SGTransformer for graph-to-layout prediction & an Image Transformer with VQVAE for layout-to-image generation. The model outperforms existing methods on Visual Genome, COCO, & CLEVR in fidelity & diversity.

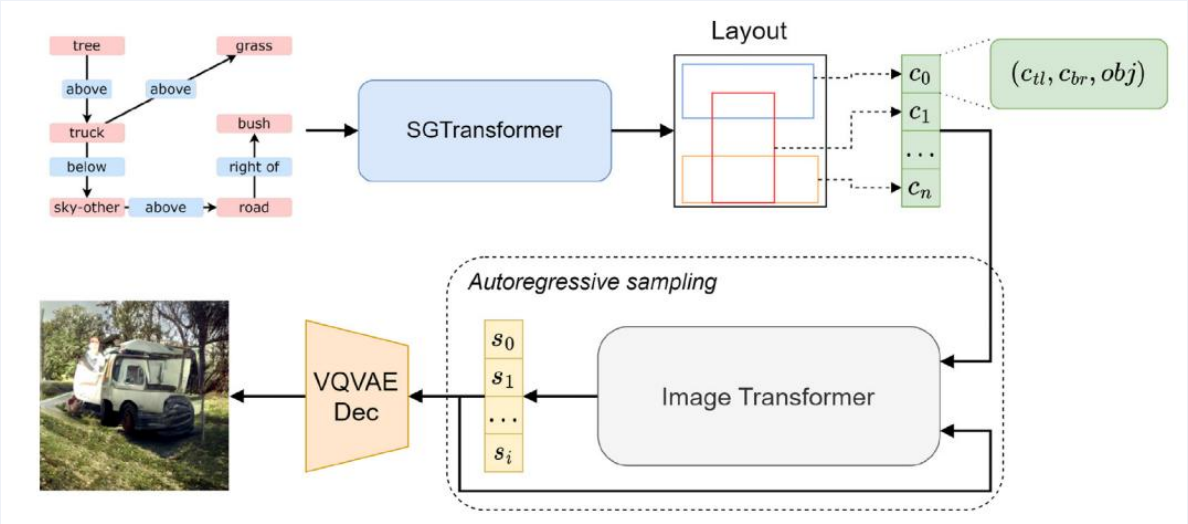

Figure 11. Overview of Framework used in[8]

Quantitative evaluations include Inception Score, FID, & mean IoU. Qualitative analyses assess layout accuracy, visual fidelity, & sample diversity. Additional ablation studies evaluate architectural choices & scene graph perturbation resilience.

Evaluating & Backing Findings

Researchers benchmarked against SG2IM, PasteGAN, & others using three datasets. Layout & image quality were measured with FID, Inception Score, & IoU. Ablation studies tested attention strategies & positional encoding, while perturbation tests validated robustness to scene graph edits.[8]

(Paper 9) This paper presents a hybrid system combining a small multi-modal model (PKATransNet) & a fine-tuned large language model (Phi-3-mini-4k) aligned via odds ratio preference optimization (ORPO) for continual radiology report generation. It achieves state-of-the-art results on IUXRAY & COVCTR datasets by reducing hallucinations & enhancing clinical accuracy.

Model	Total parameters	Trainable parameters	Trainable percentage
PKATransNet	321 M	18 M	5.61%
Phi-3-mini-4k (LoRA-32)	3.8B	50 M	1.32%
Phi-3-mini-4k (LoRA-64)	3.8B	100 M	2.63%

M stands for million, and B stands for billion

Figure 12. Screenshot of table showing Model parameters statistics [9]

Quantitative evaluation uses BLEU, METEOR, ROUGE-L, & F1-RadGraph. Qualitative analyses include ablation studies, prompt formatting tests, & visual comparisons of generated vs. reference reports.

Evaluating & Backing Findings

They benchmarked their approach against baselines, conducted ablation studies with LoRA configurations, & measured alignment effectiveness via F1-RadGraph. Visual reports & error analysis validated alignment, accuracy, & real-world applicability.[9]

(Paper 10) This work introduces GCML, a framework combining generalized clustering & multi-manifold learning while preserving geometric structure. Using a denoising autoencoder & novel loss functions (clustering, isometric, ranking, & alignment), the method achieves superior clustering accuracy & preserves both local & global structures, improving downstream task performance across diverse datasets.

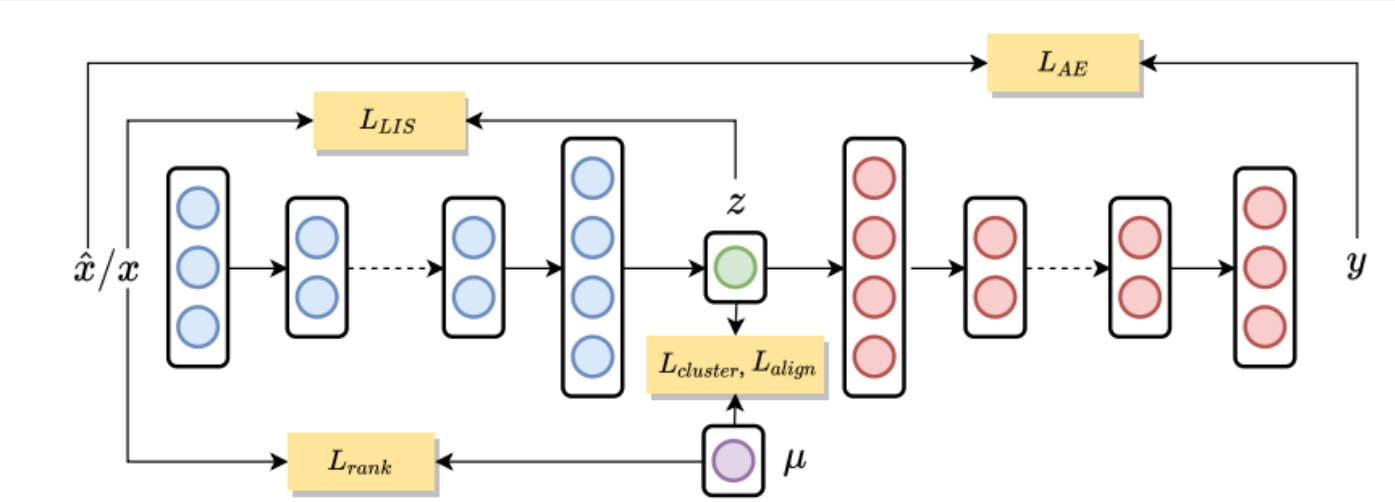

Figure.13 The GCML framework [10]

Quantitative metrics include clustering (ACC, NMI), structure preservation (Trust, Cont, CRA), & downstream classifiers (MLP, RFC, SVM, LR). Qualitative methods involve visualization & statistical analysis of latent space structure preservation during training & testing phases.

Evaluating & Backing Findings

GCML was tested on seven benchmarks. It was compared to 12 methods using accuracy, manifold preservation metrics, & classifier transferability. Embedding quality was visualized across training epochs. Statistical tests & ablation studies verified the role of each loss & training strategy. Results validated the framework's robustness & generalizability.[10]

References

[1] X. Yi, E. Walia, & P. Babyn, "Generative adversarial network in medical imaging: A review," *Med. Image Anal.*, vol. 58, no. 101552, p. 101552, 2019. https://doi.org/10.1016/j.media.2019.101552

[2] M. J. M. Chuquicusma, S. Hussein, J. Burt, & U. Bagci, "How to fool radiologists with generative adversarial networks? A visual turing test for lung cancer diagnosis," in *2018 IEEE 15th International Symposium on Biomedical Imaging (ISBI 2018)*, 2018. 10.1109/ISBI.2018.8363564

[3] M. Frid-Adar, E. Klang, M. Amitai, J. Goldberger, & H. Greenspan, "Synthetic data augmentation using GAN for improved liver lesion classification," in *2018 IEEE 15th International Symposium on Biomedical Imaging (ISBI 2018)*, 2018. 10.1109/ISBI.2018.8363576

[4] S. Kazeminia *et al.*, "GANs for medical image analysis," *Artif. Intell. Med.*, vol. 109, no. 101938, p. 101938, 2020. https://doi.org/10.1016/j.artmed.2020.101938

[5] M. Usman Akbar, M. Larsson, I. Blystad, & A. Eklund, “Brain tumor segmentation using synthetic MR images - A comparison of GANs & diffusion models,” *Sci. Data*, vol. 11, no. 1, p. 259, 2024. https://doi.org/10.1038/s41597-024-03073-x

[6] A. L. Y. Hung *et al.*, “Med-cDiff: Conditional medical image generation with diffusion models,” *Bioengineering (Basel)*, vol. 10, no. 11, p. 1258, 2023. **https://doi.org/10.3390/bioengineering10111258**

[7] R. Lin, C. Li, & R. Wang, “A benchmark for multi-task evaluation of pretrained models in medical report generation,” *BIO Web Conf.*, vol. 174, p. 03010, 2025. https://doi.org/10.1051/bioconf/202517403010

[8] R. Sortino, S. Palazzo, F. Rundo, & C. Spampinato, “Transformer-based image generation from scene graphs,” *Comput. Vis. Image Underst.*, vol. 233, no. 103721, p. 103721, 2023. https://doi.org/10.1016/j.cviu.2023.103721

[9] A. Izhar, N. Idris, & N. Japar, “Engaging preference optimization alignment in large language model for continual radiology report generation: A hybrid approach,” *Cognit. Comput.*, vol. 17, no. 1, 2025. https://doi.org/10.1007/s12559-025-10404-6

[10] L. Wu, Z. Liu, J. Xia, Z. Zang, S. Li, & S. Z. Li, “Generalized clustering & multi-manifold learning with geometric structure preservation,” in *2022 IEEE/CVF Winter Conference on Applications of Computer Vision (WACV)*, 2022, pp. 1668–1676. 10.1109/WACV51458.2022.00173

[11] F. Beck, S. Koch, and D. Weiskopf, “Visual analysis and dissemination of scientific literature collec tions with SurVis,” IEEE Trans. Vis. Comput. Graph., vol. 22, no. 1, pp. 180–189, 2016. http://dx.doi.org/10.1109/TVCG.2015.2467757